

MIMO-OFDM FOR A CELLULAR DEPLOYMENT - CONCEPTS, REAL-TIME IMPLEMENTATION AND MEASUREMENTS TOWARDS 3GPP-LTE

T. Haustein, J. Eichinger, W. Zirwas, E. Schulz
Nokia Siemens Networks GmbH & Co.KG,
St. Martinstraße 76, 81617 Munich

A. Forck, H. Gäbler, V. Jungnickel, S. Wahls,
Fraunhofer Heinrich Hertz Institute,
Einsteinufer 37, 10587 Berlin

C. Juchems, F. Luhn,., Zavrtak,
IAF GmbH, Berliner Str. 52 J,
38104 Braunschweig

Invited Paper

ABSTRACT

In this paper we report on the system design and a real-time implementation of a MIMO-OFDM radio transmission system close to physical layer parameters as discussed in standardization for 3GPP-Long-Term-Evolution. We describe the implementation concept and first results on over-the-air transmission with a single user set-up occupying 20 MHz bandwidth and achieving more than 150 Mbit/s gross data rate in the 2x2 MIMO down-link and more than 50 Mbit/s in the single transmit antenna up-link. The demonstration system was only recently shown to the public at various trade shows like ITU in Hongkong and 3GSM in Barcelona.

1. INTRODUCTION

The increasing demand for improvements in cellular radio communications is reflected in discussions of many standardization bodies like 3GPP which try shape the evolution of the current UMTS system. The current system proposal also known as 3GPP-Long-Term-Evolution (LTE) already agreed on many working assumptions for further evaluation of the system design in order to improve the final decisions going into the standard for commercialization. Starting from basic physical layer assumptions agreed around November 2005 a demonstration system was planned to allow early evaluation of aspects of the LTE-standard and feed-back into the standardization body.

The first design focussed on PHY issues of the MIMO-OFDM system including synchronization, channel estimation, signal separation and basic features of link adaptation and was implemented on a similar signal processing hardware platform as used for the 1 Gigabit/s experiment [1].

The transmission band was chosen in the UMTS extension band at 2.6 GHz with two FDD bands of 20 MHz each,

at a spacing of 150 MHz. The RF front-ends include duplex filters, mixers, local oscillators and automatic gain control and allow MIMO-OFDM transmission up-to 64-QAM in the Uplink and Downlink while satisfying spectral emission mask requirements. The connection between RF front-end and the base band processing unit was realized via CPRI and LVDS interface adopted to 20 MHz bandwidth. The bandwidth can be set to 20 / 10 / 5 MHz in the digital domain.

In this paper we will focus on the base band processing of the LTE demo system. We will describe the general structure of the applied PHY layer with the belonging parameters and will discuss challenges regarding efficient implementation in more details. Finally we will present first measurement results on a single user setup using fast channel adaptive link adaptation in the MIMO downlink.

2. SYSTEM MODEL

We consider an OFDM system with n_T transmit antennas and a base station having m_R antennas. We assume appropriate frame and symbol synchronization. The transmission channel between all antenna pairs is a frequency selective fading channel of order L . Using OFDM techniques the channel can be decomposed into D flat sub-channels. Hence, using Fourier Transform (FFT) the received signal at k -th sub-carrier is given by a flat fading MIMO equation

$$y_k = H_k \cdot x_k + n_k \quad (1)$$

$x_k^{n_T \times 1}$ is a zero-mean transmit vector on sub-carrier k , $H_k^{m_R \times n_T}$ the k -th MIMO channel matrix and $n_k^{m_R \times 1}$ is circular symmetric zero-mean additive white Gaussian noise with expectation σ_N^2 . A cyclic prefix (CP) of length $L_{CP} > L$ assures orthogonality between OFDM symbols.

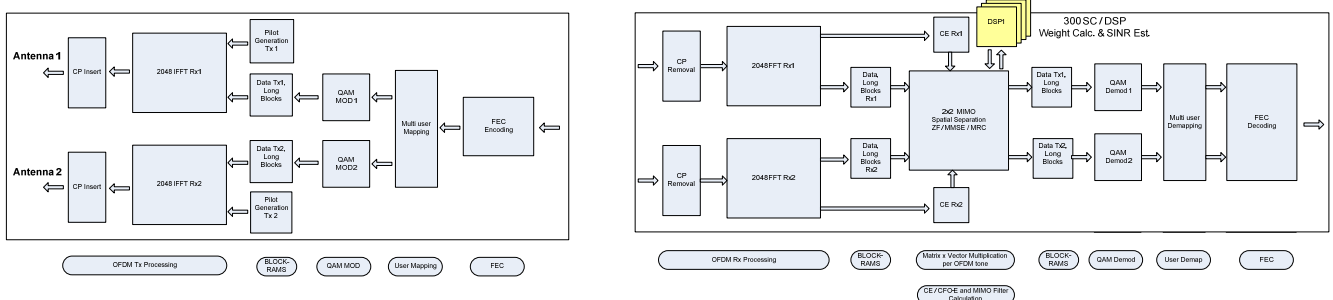


Figure 1: Functional blocks of the down-link base band chain. Left: Transmitter at BS; Right: Receiver at one UE

Report Documentation Page				Form Approved OMB No. 0704-0188	
Public reporting burden for the collection of information is estimated to average 1 hour per response, including the time for reviewing instructions, searching existing data sources, gathering and maintaining the data needed, and completing and reviewing the collection of information. Send comments regarding this burden estimate or any other aspect of this collection of information, including suggestions for reducing this burden, to Washington Headquarters Services, Directorate for Information Operations and Reports, 1215 Jefferson Davis Highway, Suite 1204, Arlington VA 22202-4302. Respondents should be aware that notwithstanding any other provision of law, no person shall be subject to a penalty for failing to comply with a collection of information if it does not display a currently valid OMB control number.					
1. REPORT DATE SEP 2007		2. REPORT TYPE N/A		3. DATES COVERED -	
4. TITLE AND SUBTITLE MIMO-OFDM for a Cellular Deployment - Concepts, Real-Time Implementation and Measurements Towards 3GPP-LTE				5a. CONTRACT NUMBER	
				5b. GRANT NUMBER	
				5c. PROGRAM ELEMENT NUMBER	
6. AUTHOR(S)				5d. PROJECT NUMBER	
				5e. TASK NUMBER	
				5f. WORK UNIT NUMBER	
7. PERFORMING ORGANIZATION NAME(S) AND ADDRESS(ES) Nokia Siemens Networks GmbH & Co.KG, St. Martinstraße 76, 81617 Munich				8. PERFORMING ORGANIZATION REPORT NUMBER	
9. SPONSORING/MONITORING AGENCY NAME(S) AND ADDRESS(ES)				10. SPONSOR/MONITOR'S ACRONYM(S)	
				11. SPONSOR/MONITOR'S REPORT NUMBER(S)	
12. DISTRIBUTION/AVAILABILITY STATEMENT Approved for public release, distribution unlimited					
13. SUPPLEMENTARY NOTES See also ADM002358. European Signal Processing conference (15th) (EUSIPCO 2007) Held in Poznan, Poland on September 3-7, 2007. U.S. Government or Federal Purpose Rights License., The original document contains color images.					
14. ABSTRACT In this paper we report on the system design and a realtime implementation of a MIMO-OFDM radio transmission system close to physical layer parameters as discussed in standardization for 3GPP-Long-Term-Evolution. We describe the implementation concept and first results on over-the-air transmission with a single user set-up occupying 20 MHz bandwidth and achieving more than 150 Mbit/s gross data rate in the 2x2 MIMO down-link and more than 50 Mbit/s in the single transmit antenna up-link. The demonstration system was only recently shown to the public at various trade shows like ITU in Hongkong and 3GSM in Barcelona.					
15. SUBJECT TERMS					
16. SECURITY CLASSIFICATION OF:			17. LIMITATION OF ABSTRACT SAR	18. NUMBER OF PAGES 5	19a. NAME OF RESPONSIBLE PERSON
a. REPORT unclassified	b. ABSTRACT unclassified	c. THIS PAGE unclassified			

3. MIMO-OFDM DOWNLINK

The parameter set for the PHY implementation was chosen according to working assumption around November 2005. For the downlink we use 2 transmit antennas at the base station (BS) and 2 receive antennas at the user equipment (UE). In the targeted 20 MHz mode the FFT/IFFT size is 2048 points with 48 resource blocks (RBs) each containing 25 sub-carriers (SC) and 7 long OFDM symbols (TTI) with 1200 SCs each. The cyclic prefix / guard interval was 4.7 μ s. 20 consecutive TTIs form a radio transmission frame of 10 ms.

3.1 Channel Estimation Down-link

3.1.1 MIMO Channel Estimation

The reference symbols per transmit antenna in the DL use known scrambled PBSK symbols equidistantly distributed in frequency domain per RB (7 pilot per 25 sub-carriers) and the two transmit antennas are separated in the code-domain over time [1]. The channel estimates are collected after FFT in the FPGA. The channel between the estimated pilots is interpolated in a DSP cluster using a complexity reduced algorithm [2] which performs close to Wiener filtering. This interpolation technique also allows a precise signal-to-noise-ratio estimation which is averaged for each Rx antenna. For temporal interpolation dedicated phase tracking pilots at various positions in the spectrum are used.

3.1.2 Frequency and Time Synchronization

A coarse frequency estimation is performed at the UE in front of the FFT based on a special pre-amble transmitted in TTI 0. The remaining centre frequency offset between the BS and the UE is measured in the frequency domain after FFT exploiting the dedicated phase tracking pilots from the channel estimation and MRC detection. Using different loop feedback the remaining CFO can be reduced down to a few 10 Hz in a static environment at SNR above 10 dB.

The OFDM frame sync is based on another special pre-amble using a Schmidl-Cox correlator before FFT at the UE. For the current single user / close range scenario no timing advance estimation and compensation is implemented.

3.2 Spatial Signal Separation

The spatial separation of the data signals transmitted from the two antennas is performed inside the FPGA in the fre-

quency domain after FFT per sub-carrier based on MIMO processing while the MMSE [3] or MRC filter weights per sub-carrier are calculated in the DSP every 500 μ s.

Furthermore, the SNR [2] per chunk is estimated and made available to the Viterby-decoder for soft decoding.

Due to the stringent timing requirements of calculating 1200 2x2 MIMO matrices every 500 μ s we decided for a DSP star architecture using 4 floating point DSPs TI 6713 each processing 300 SCs.

3.3 Link Adaptation

One important advantage of OFDM compared to CDMA techniques that it can exploit frequency dependent resource allocation with specific Modulation and Coding Scheme (MCS) levels for each RB allocated for a specific user.

Depending on the applied MIMO detection scheme at the receiver the effective SINR in front of the demodulator is calculated and used as input for an adaptive bit-loading algorithm. For the current single user setup the link adaptation including MIMO mode selection and adaptive bit-loading is performed at the UE and a new chunk allocation vector is transmitted to the BS via a dedicated PDU which is protected with CRC, 1/2 rate coding, BPSK and diversity reception using MRC at the BS.

By this very basic link adaptation loop we achieve full flexibility in antenna positions even with the 2x2 antenna configuration. Our measurements show link adaptation in the 2x2 MIMO down-link while the up-link is operated with fixed MCS and resource allocation exploiting cyclic delay diversity (CDD) at the UE and MRC at the BS.

4 SC-FDMA UPLINK

At the current demo system the up-link TTI consists of 6 long OFDM symbols (LB) with 1200 SCs and 2 short OFDM symbols with 600 SCs at positions 2 and 7 for channel estimation in an OFDM fashion.

The parameter set for the PHY implementation was chosen according to working assumption around November 2005. For the downlink we use 2 Tx antennas at the base station (BS) and 2 Rx antennas at the user equipment (UE). In the 20 MHz mode the FFT/IFFT size is 2048 points with 48 resource blocks (RBs) each containing 25 sub-carriers (SC) and 7 long OFDM symbols (TTI) with 1200 SCs each. The cyclic prefix / guard interval was 4.7 μ s. 20 consecutive TTIs form a radio transmission frame of 10 ms.

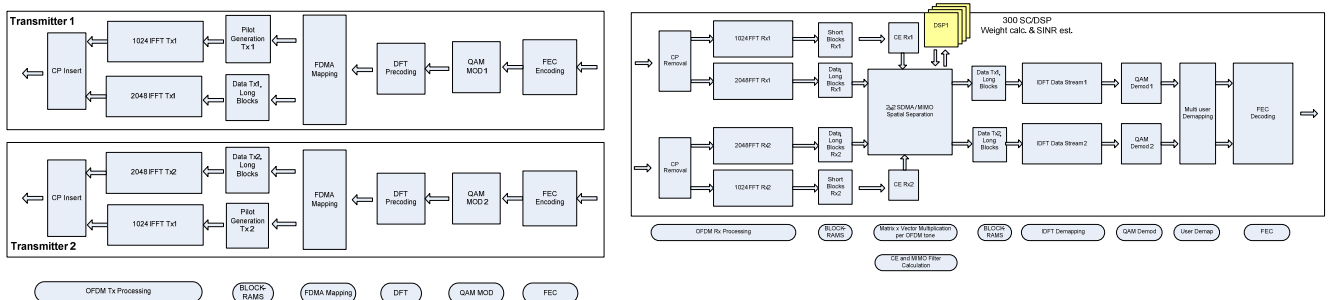


Figure 2: Functional blocks of the up-link chain. Left: 2 transmitters of 2 UEs, Right: Multi-user receiver at one the BS

4.1. Channel Estimation Up-link

4.1.1 Channel Estimation in the up-link

In a FDMA based multi-user scenario in principle each RB can be allocated to a different user in the up-link. Therefore, the pilot structure was defined locally within each RB. For the case of spatial multiplexing in the up-link the multiple transmit antennas have to use orthogonal pilot patterns to be distinguishable. Due to the fact that one pilot in the SB represents every second sub-carrier in the LB the choice of 25 SC per RB is unfavourable (meanwhile standardization has decided 12 SCs per RB which corresponds to exactly 6 SCs in the SB). Considering this we combined 2 RBs of 25 SCs each two a double RB which is considered in the resource allocation scheduler.

For the current single user case with maximum two Tx antennas at the UE we omit a special broadband measurement pilot sequence and allow the two Tx antennas to transmit the same pilot patterns in all RBs.

4.1.2 Temporal Phase Estimation

The channel estimates collected at the FPGA in the BS are given to the DSPs which perform channel interpolation in the time and frequency domain. Keeping in mind a possible MIMO configuration in the uplink for SDMA we can perform the channel estimation in four steps:

1. Perform de-scrambling over the frequency domain.
2. Calculate the phase evolutions ϕ_1 and ϕ_2 on SCs which have a pilot in both SBs of each Tx antenna, respectively, in order to compensate Doppler and remaining CFO per Tx antenna. Average over all available phase tracking pilots. The estimation can be improved with MRC if the Doppler is reasonably small.
3. Combine the estimates of the first and the second SB using an inverse phase shift $e^{-i\phi_1}$ according to :

$$\tilde{H}_k^{jl}(SB1) = \frac{1}{2} (H_k^{jl}(SB1) + H_k^{jl}(SB2) \cdot e^{-i\phi_1}) \cdot F_k$$

If $H_k^{jl}(SB1) = 0$ or $H_k^{jl}(SB2) = 0$ then $F_k = 2$ else $F_k = 1$

4. Interpolate the MIMO channels for each antenna pair \tilde{H}_k^{jl} .

In order to benefit from frequency interpolation we decided for a precise phase measurement in the centre and a closer sample grid at the edges of each RB.

4.2 Spatial Signal Separation

Like in the down-link four DSPs calculate and write the MRC filter weights and the phase evolution factors back to the FPGA which performs a matrix vector multiplication between the received signal vectors and the spatial filter matrix/vector per SC.

After the spatial separation remaining phase rotations will be seen between consecutive OFDM symbols. These phase rotations are compensated by the interpolated phase factors measured for the Tx antennas. This technique showed

a significant reduction in phase variations which may come from independent phase noise between the local oscillators at the UEs and the BS, residual CFO errors from independent CFO measurement and pre-compensation at each UE and from time-variant Doppler.

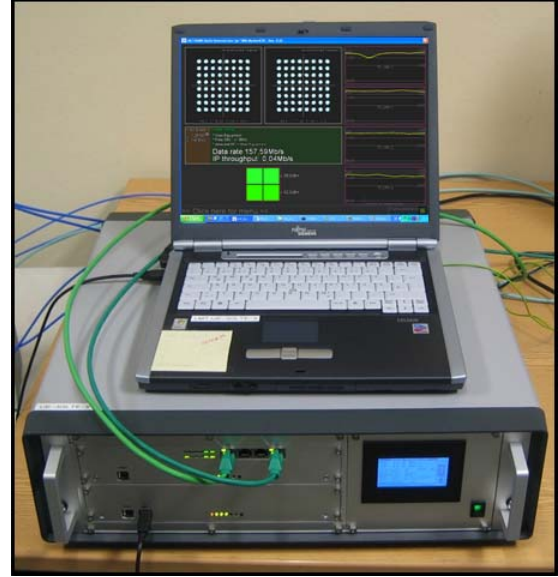


Figure 3: User Equipment with Local Monitoring Terminal (LMT) showing reconstructed signal constellations, channel transfer functions, throughput, BER, CFO etc.

4.3 Pulse Shaping with DFT Pre-coding

4.3.1 DFT pre-coding and IDFT decoding

In order to reduce the peak-to-average-power-ratio (PAPR) especially for cell-edge users 3GPP-LTE agreed on DFT pre-coding at the UE and a matching IDFT at the BS. The resulting signal envelope shows a significant reduced PAPR especially for low order modulation levels e.g. BPSK and QPSK compared to standard OFDM.

For the demo system we focused on localized sub-carrier allocation [4], nevertheless distributed sub-carrier allocation similar to IFDMA can also be supported with slight changes in the sub-carrier mapping module which in the localized mode maps the DFT pre-coded symbols to adjacent sub-carriers in the frequency domain.

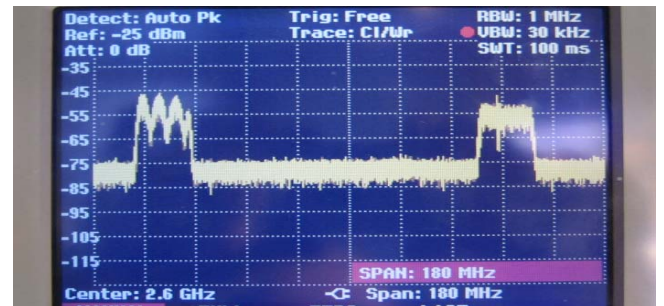


Figure 4: Transmission spectrum at 2.6 GHz. with 150 MHz spacing between up-link (left) and down-link (right). The left spectrum shows the typical characteristics of a CDD.

5 DOWNLINK EXPERIMENTS ON MIMO-OFDM

First experiments were conducted in a typical indoor office environment in order to verify the performance of channel estimation and MIMO detection for a single user scenario.

We focussed primarily on the down-link using 2x2 MIMO and link adaptation while the up-link was operated in a robust 1x2 SIMO scheme with MRC at the receiver.

In order to validate the system under operation a specially prepared Local Monitoring Terminal (LMT) was writing measured data sets like channel state information, SINR, AGC-values, achieved BER with and w/o coding and bit-loading information from the link adaptation into log files.

From the log files we extracted plots over time and frequency which will be discussed in the following. The system performance of the RF and the base band was pre-checked in a two cable link supporting modulation schemes from BPSK to 64-QAM with an un-coded bit error rate (BER) below 10^{-5} .

A first prediction about the statistical properties in the transmission scenario can be derived from the singular value (SV) distribution depicted in Fig. 6, note that all channel were normalized to allow comparison with simulations. Here, the long tail of SV2 to very small values indicates that spatial multiplexing will sometimes not be supported due to the resulting variation in the achievable SINR at the demodulator. This is a direct consequence from the lack of spatial diversity with the 2x2 symmetric antenna configurations. Exploiting link adaptation including adaptive MIMO mode and MCS selection should enable us to benefit significantly from the rich scattering multi-path environment found in the office scenario. Very similar results were already reported with 100 MHz bandwidth at 5 GHz carrier frequency [3] and omni-directional antennas at both sides of the link.

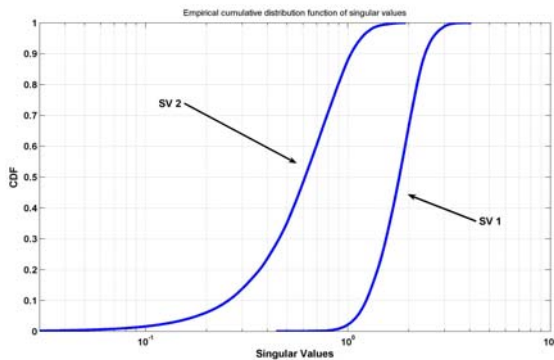


Figure 5: Cdfs of the singular values during the experiments in the 2x2 MIMO downlink in 20 MHz bandwidth, channels normalized.

System Setup:

The base station (BS) transmit antennas were placed in a corner of the office facing the diagonal of the room. The BS antennas used cross polarized sector antennas while the UE used omni-directional antennas also with cross polarization. The transmit power was about 10dBm per Tx antenna using a fixed power per sub-carrier¹.

¹ No power loading per RB was applied, meaning that if one RB is in single stream mode the saved power could not be allocated to another RB. This

The UE together with its antennas was put on a little trolley and moved through the lab. The sum rate maximizing bit-allocation was calculated at the UE and signalled over the uplink control channel.

5.1. SINR Distribution over space and frequency

The SINR plots in Fig. 6 lead to the following conclusions:

1.) The reception quality of the two transmit antennas is almost balanced over the measurement scenario and spatial multiplexing can be supported quite often along the measurement track. One Tx antenna is favoured due to one Rx antenna with a similar polarization is pointing to the BS.

2.) The use of a linear MMSE detector for the 2x2 spatial multiplexing achieves a SINR variation from 30 dB between the worst and the best channels. Due to the exploited cross polarization with sector antennas at the BS side and cross polarized omni-directional antennas at the UE the gain in achievable SINR between MMSE and ZF is limited to the very bad conditioned channels and has therefore little impact on the throughput at high SNR. Nevertheless, in outdoor scenarios especially at low SNR and non-perfect cross polarization at one or both of the transmission ends MMSE provides more robustness regarding BER performance in non-frequency adaptive transmission schemes and higher throughput with link adaptation.

3.) MRC improves the achievable SINR for each Tx antenna at the cost of throughput multiplexing. The tail to small SINR values is significant shorter. Note that by choosing always the better of the two Tx antennas and the belonging MRC detector allows a significant reduction of the outage probability at lower SINR values and thus virtually enables us to force a certain minimum SINR on all RBs which allows for easy and persistent scheduling.

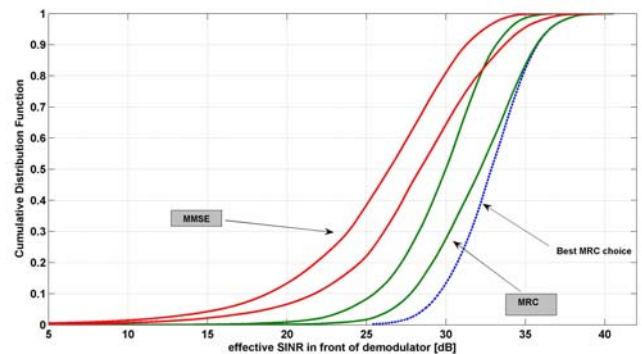


Figure 6: Cdfs of the achievable SINRs during the link adaptation experiments in a scenario with similar receive power per Rx antenna in the 2x2 MIMO downlink assuming MRC for either Tx 1 or Tx 2, best MRC choice and linear MMSE as detection schemes which also shows the effective SINR for Tx 1 and Tx 2.

5.2. Measured Throughput with Link Adaptation

Fig. 7 shows the received power at the UE antennas, the achieved throughput with link adaptation when moving the

approach goes well with the assumption of a constant inter-cell interference situation as long as the beamformers in neighbouring cells are not changed.

UE through the office and the resulting uncoded BER. The link adaptation including MIMO mode selection and MCS selection (with fixed code rate) was adapted every radio frame (10 ms). From the logged bit-loading pattern per transmit antenna we calculate the achieved throughput within one TTI of 500 μ s per transmit antenna from the MCS used in each RB (Note that 144 symbols per RB carry data.)

$$\text{Rate at Tx}_{1,2} \rightarrow R = \sum_{k=1}^{48} \text{Mod}(\text{RB}_k) \text{bits} \cdot 144 / 500 \mu\text{s}$$

The results in Fig. 7 show the throughput for each Tx antenna considering a factor of 19/20 since TTI-0 was excluded from data transmission.

From the top plot in Fig. 7 we observe that one Rx antenna “red” receives always about 5 to 10 dBs less power than the second Rx antenna. This is easily explained by the fact that one antenna points more towards the BS and the other more to the wall. This situation is a natural situation for a multi-antenna system with more or less arbitrary antenna positions in the room. In our indoor experiments the received broadband power within 20 MHz bandwidth for the two Rx antennas rarely differed by more than 10 dB due to the strong NLOS component, but for a cellular outdoor scenario this difference is expected to be significant higher.

The measurement track consisted of the first 60% of sample points² measured within the main lobe of the BS antennas while the UE moved from about 25 meters start distance between UE and BS to almost 5 meters before the main lobe is left (LOS \rightarrow NLOS). Although the received power stays almost the same the rate drops significantly, since the channel rank decreases for many RBs in the 2x2 antenna configuration. At about time slot 350 we leave the office through a door and continue behind a wall of steel cupboards. The received power drops by about 10 dB, when leaving the office. Due to the higher received power from Tx antenna 1 (blue color) the scheduler starts to favour this antenna on all RBs for certain UE positions. This can be seen where the sum throughput for the “red” Tx antenna drops to zero.

The measured average sum gross throughput for the single UE using the full bandwidth and spatial multiplexing when possible was above 120 Mbit/s in the high SNR indoor scenario with a maximum rate of 157 Mbit/s when all RBs on the two Tx antennas used 64-QAM. Depending on the chosen code rate (e.g. 3/4) a net throughput above 100 Mbit/s could be realized as targeted by 3GPP.

The bottom plot shows the uncoded BER when exploiting fast link adaptation. The target BER was set to 10^{-3} to ensure error free transmission after forward error correction.

6 CONCLUSIONS

In this paper we showed the feasibility of a real-time implementation of a new air-interface with similar PHY parameters as discussed in 3GPP-LTE using MIMO-OFDM on a

reconfigurable hardware test-bed. First experiments with a single user showed net peak rates above 100 Mbits/s in very good channels and robust transmission when combined with basic link adaptation functionalities in the down-link.

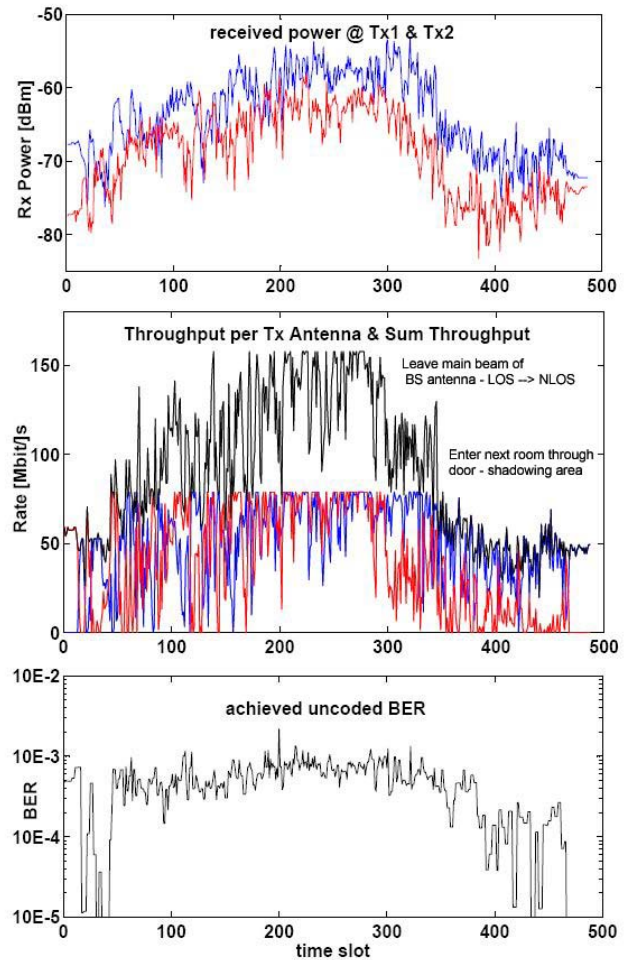


Figure 7: Plots of received power (top), throughput (middle) and BER (bottom) in an office scenario while the UE is moved from one room to another.

REFERENCES

- [1] V. Jungnickel, A. Forck, T. Haustein, C. Juchems and W. Zirwas, „Gigabit Mobile Communications Using Real-Time MIMO-OFDM Signal Processing“, chapter 11 in MIMO Systems Technology for Wireless Communications.
- [2] S. Schiffermüller, V. Jungnickel, “Practical Channel Interpolation for OFDMA”, IEEE Globecom 2006, San Francisco, USA, 27.11.-2.12.2006
- [3] T. Haustein, A. Forck, H. Gäbler, V. Jungnickel and S. Schiffermüller, „Real-Time Experiments on Channel Adaptive Transmission in the Multi-User Up-link at very high Data Rates using MIMO-OFDM“, EUSIPCO 2006, Florence, Italy, Sept. 2006
- [4] V. Jungnickel, T. Hindelang, W. Zirwas and T. Haustein „SC-FDMA Waveform Design, Performance, Power Dynamics and Evolution to MIMO“, IEEE Portable, 25.-27. March 2007, Orlando, Florida, USA
- [5] 3GPP Long Term Evolution standardization working documents 36.212, 36.213, 36.214 to be found at www.3gpp.org/ftp/Specs/...

² The sample points were taken every 300 ms with an average BER measurement over this time and a slow movement through the room. Therefore the located bit-loading pattern does not vary much over the 300 ms.